

Review

Catalytic Hydrogen Production from Methane: A Review on Recent Progress and Prospect

Luning Chen ^{1,†}, Zhiyuan Qi ^{1,†}, Shuchen Zhang ¹ , Ji Su ^{1,2,*} and Gabor A. Somorjai ^{1,3,*}

¹ Materials Sciences Division, Lawrence Berkeley National Laboratory, Berkeley, CA 94720, USA; luningchen@lbl.gov (L.C.); zhiyuan7@lbl.gov (Z.Q.); shuchenzhang@lbl.gov (S.Z.)

² Molecular Foundry, Material Science Division, Lawrence Berkeley National Laboratory, Berkeley, CA 94720, USA

³ Department of Chemistry, University of California-Berkeley, Berkeley, CA 94720, USA

* Correspondence: jisu@lbl.gov (J.S.); somorjai@berkeley.edu (G.A.S.); Tel.: +1-(510)-642-4053 (G.A.S.)

† These authors contributed equally to this work.

Received: 20 July 2020; Accepted: 30 July 2020; Published: 2 August 2020



Abstract: Natural gas (Methane) is currently the primary source of catalytic hydrogen production, accounting for three quarters of the annual global dedicated hydrogen production (about 70 M tons). Steam–methane reforming (SMR) is the currently used industrial process for hydrogen production. However, the SMR process suffers with insufficient catalytic activity, low long-term stability, and excessive energy input, mostly due to the handling of large amount of CO₂ coproduced. With the demand for anticipated hydrogen production to reach 122.5 M tons in 2024, novel and upgraded catalytic processes are desired for more effective utilization of precious natural resources. In this review, we summarized the major descriptors of catalyst and reaction engineering of the SMR process and compared the SMR process with its derivative technologies, such as dry reforming with CO₂ (DRM), partial oxidation with O₂, autothermal reforming with H₂O and O₂. Finally, we discussed the new progresses of methane conversion: direct decomposition to hydrogen and solid carbon and selective oxidation in mild conditions to hydrogen containing liquid organics (i.e., methanol, formic acid, and acetic acid), which serve as alternative hydrogen carriers. We hope this review will help to achieve a whole picture of catalytic hydrogen production from methane.

Keywords: hydrogen economic; methane conversion; heterogeneous catalysts

1. Introduction

Methane (CH₄) is an important chemical feedstock for hydrogen production. In the United States, more than 95% of the hydrogen is produced by steam–methane reforming (SMR) with an annual hydrogen production of 10 million metric tons. SMR is a mature industrial process to harvest H₂ from a methane source (e.g., natural gas) under high-temperature steam (700–1000 °C) with a pressure range of 3–25 bar. Besides H₂, carbon monoxide (CO), and a relatively small amount of carbon dioxide (CO₂) were also obtained from SMR, which was therefore developed to manufacture syngas (H₂ and CO) traditionally. When coupled with a water–gas shift (WGS) reaction, the co-product CO from SMR could further react with steam to result in one extra H₂ and CO₂ as the final products [1–3]. In general, SMR could be considered as a catalytic process that accelerates the decomposition of methane to H₂ gas and carbon species. The C species were then further reacted with oxygen via a gasification reaction to generate CO/CO₂ and recover the active sites.

Although SMR is a mature technology, it still suffers from several disadvantages caused by the reactant properties and reaction thermodynamics: High energy consumption, high production cost, harsh reaction conditions, low reaction efficiency, and low process stability [4,5]. Specifically,

the disadvantages are mainly reflected in three aspects: Firstly, methane is very stable, and thus hard to activate. Due to the highly endothermic nature ($\Delta H_o = 206$ kJ/mol), SMR requires extra energy and designed instruments to proceed the reaction at high temperature and pressure, which also introduces mass transfer and heat transfer issues. Secondly, the design of catalysts still needs improvement. On the one hand, noble metal catalysts (e.g., Ru, Rh) displayed high SMR activities with good stability. However, the cost and availability of noble metals limit their application [6–8]. On the other hand, the commercial catalyst Ni/Al₂O₃ suffers serious deactivation, due to the easy sintering and coke formation of Ni catalysts. Thirdly, SMR coproduces CO₂, especially when coupled with a WGS for H₂ production (9–14 kg CO₂/kgH₂). The CO₂ has a strong greenhouse effect and its handling further increases the cost of the SMR process [9].

To develop a highly efficient, low cost and stable methane reforming process, the research effects focus on three directions. First of all, alternative and upgraded techniques for methane conversion were developed including dry reforming with carbon dioxide (DRM) [10–12], partial oxidation with O₂ [13,14], autothermal reforming with H₂O and O₂ [15], low temperature SMR [16], combined steam and dry reforming of methane (CSDRM) [17], a chemical looping SMR process (CL-SMR) [18], a sorption-enhanced SMR (SE-SMR) [19–21], as well as a combined CL-SE-SMR process [22]. Each process generates a syngas mixture with an alternating H₂:CO ratio, due to different reaction conditions applied such as temperature and pressure. Furthermore, a series of catalysts with higher activity and stability were designed and fabricated. The most investigated catalysts in this field are mostly from Group VIII, including monometallic, bimetallic noble and non-noble metal catalysts [1]. The applied metals [23], size effect [24–27], promoter effect [1,28], support effect [29–31], as well as coordination state [32] and acidic/basic properties [33] of these catalysts were studied in-depth. The catalysts applied and above-mentioned variables are essential for the control of the reaction routes and the production distributions. Finally, reaction conditions and various engineering factors of these methane reforming processes were further optimized, for example, temperature, pressure, feeding rate, feedstock ratio, reactor types etc.

2. Descriptors of Structure–Activity Relationship of the Catalyst

The descriptors of the structure–activity relationship of the catalyst such as metal type, metal coordinate state, size effect, support effect, and promoters, are an important interface to bridge the gap between deep learning and observed catalytic performance. Previous research work reveals that both SMR and DRM are structure sensitive [34–36]. Clearly, atoms with different chemical environments in the catalytic metal nanoparticles have distinct activities [24]. Therefore, mapping this structure sensitivity and understanding the associated mechanism provides opportunities to design more efficient and stable catalysts.

2.1. Metal Type Effect

One major type of steam reforming catalysts is noble metal-based. Unlike commercial Ni catalysts that have serious coking problem caused by the formation, diffusion, and dissolution of carbon in Ni metals, noble metals yield much less coking due to the difficulties of dissolving carbon in them [37]. Noble metals such as Ru, Rh, Pd, Ir, and Pt were examined for their reforming performance, among which Ru and Rh displayed high reforming activities and low carbon formation rates [38,39]. Jones et al. [25] proposed the SMR activity order as Ru > Rh > Ir > Pt, indicating Pt catalyst as the least active among the other metals. In contrast, the study of Wei and Iglesia [26] showed that C–H bond activation by Pt is more efficient than Ir, Rh, and Ru (Figure 1). Therefore, due to the disagreement from different research groups involved in this field, it is still not possible to give a specific order of catalytic activity and selectivity towards hydrogen production via SMR.

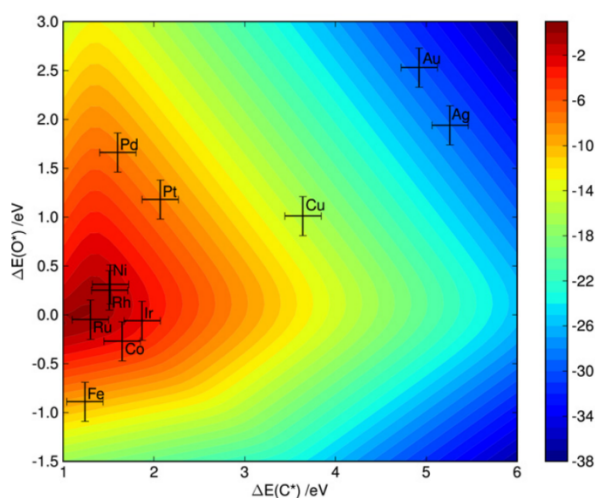


Figure 1. Two-dimensional volcano-curve of the turn over frequency (\log_{10}) as a function of O and C adsorption energy. $T = 773$ K, $P = 1$ bar; 10% conversion. The error bars include an estimated 0.2 eV uncertainties in the adsorption energies [26].

Although all these noble metal catalysts show high catalytic activity and less coke formation, the high cost hinders their practical applications. Group VIII non-noble metals are also active for SMR [40–42]. However, iron will be rapidly oxidized under reaction conditions while cobalt cannot withstand the partial pressures of steam. Therefore, nickel-based catalysts are the most studied and commonly used SMR catalysts at industrial scale mostly owing to their low cost.

2.2. Ni Size Effect

In this section, we will mainly summarize the size effect of Ni catalysts [43], considering the commercialization and extensive research work on Ni (60% of publications in the field of SMR are about Nickel catalysts [1]). The optimal Ni particle size for both SMR and DMR at 500 and 600 °C under 5 bar, was found to be approximately 2–3 nm, whereas carbon whisker formation was found to significantly occur on ~4.5 nm Ni particles during SMR and increased with increasing particle size during DRM [24].

Furthermore, the performances of single site Ni₁/MgO catalysts for DRM reaction was systemically studied by combining theoretical modeling (Density Functional Theory (DFT) and Kinetic Monte Carlo Method (KMC) simulations) and experimental results. The DFT calculations show that synergistic effect between Ni single atom and MgO support in Ni₁/MgO is not strong due to the weak binding of reaction intermediates and the limited numbers of neighboring active sites. When slightly increasing the Ni size, the single site Ni₄/MgO catalyst is able to provide stronger bindings than Ni₁/MgO. It also offers enough active but isolated Ni sites working cooperatively for the activation of both CH₄ and CO₂, which produces CO, H₂ and H₂O while completely eliminating carbon deposition. The experimental observation on a 5% Ni/MgO catalyst including a Ni cluster of 3–4 Ni atoms agrees well with the calculation predictions (Figure 2) [27].

2.3. Promoter Effect

The researchers showed that the addition of second metal to a Ni-based catalyst can improve its selectivity, durability, and activity, thus limiting the typical problems of SMR including coke formation, active oxidation, sintering, and segregation [44–47]. For example, combining of the highly reactive Ni species for CH₄ activation and Fe species for water splitting, together with the resulting Ni–Fe alloy, achieved a high CH₄ conversion up to 97.5% and CO selectivity up to 92.9% at 900 °C with productivity of CO and H₂ of 9.6 and 29.0 mol kg catalyst^{−1}, respectively (on equimolar Ni–Fe catalyst) [21].

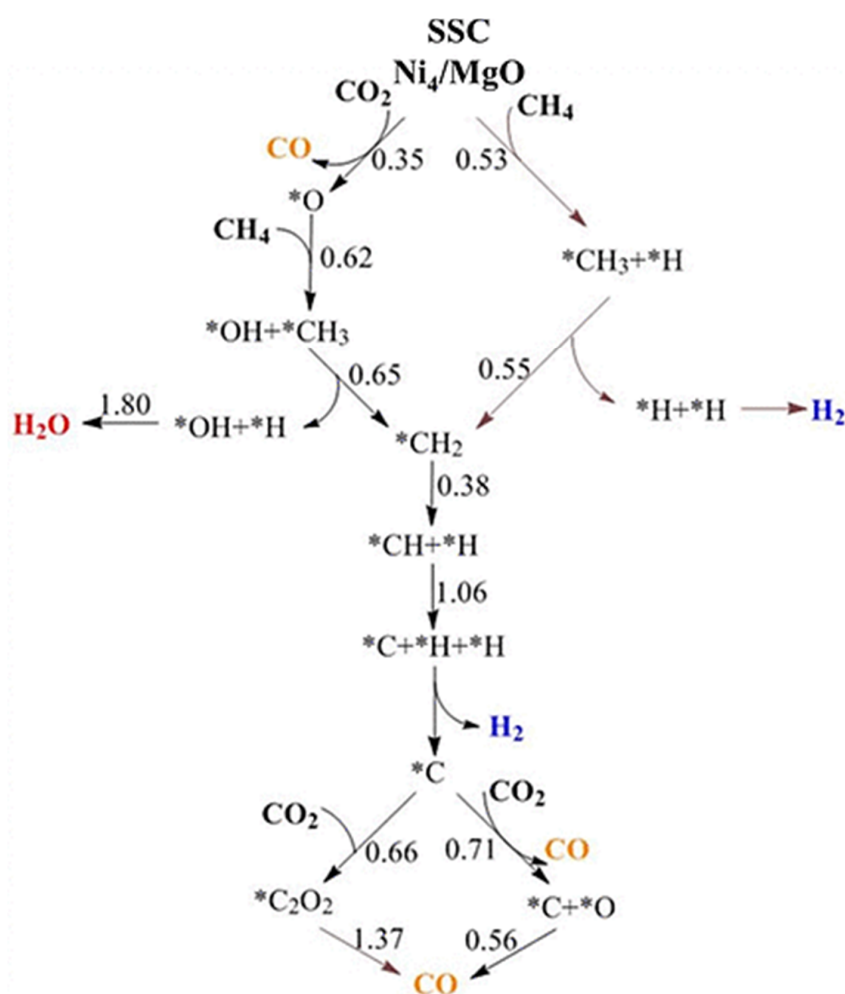


Figure 2. Schematics of KMC-identified reaction network for the dry reforming with CO₂ (DRM) on the confined single-site Ni₄/MgO(100) catalyst. The corresponding E_a for each step is also included (in eV) [27].

2.4. Support Effect

A large number of studies were focused on the improvement of Ni performance via analyzing the effect of different supports [48–51]. Nieva et al. stated that the catalytic activity of Ni-based catalysts mainly depends on the support, which plays an important role in the catalytic process. In fact, the supports influence the metal dispersion, affect sintering resistance, and sometimes directly participate in reactions by facilitating the adsorption of reactants. For SMR at 600 °C, the activity order of Ni-based catalysts with different supports was observed as: Ni/MgAl₂O₄ > Ni/ZnAl₂O₄ > Ni/Al₂O₃ > Ni/SiO₂. Specifically, Ni/SiO₂ undergoes a rapid deactivation probably due to the surface oxidation and carbon deposition, whereas Ni/ZnAl₂O₄ shows the lowest degree of carbon deposition and the highest resistance to sintering [29].

In addition, it was observed that supports such as Al₂O₃ and SiO₂ allow a gradual oxidization of Ni catalysts during SMR at 500 °C under ambient pressure, whereas the utilization of ZrO₂ stabilized Ni particles and allowed for higher methane conversion than aforementioned supports. It is mainly because the ZrO₂ support allows a water accumulation, favoring the formation of hydroxyl groups which promotes SMR [30]. CeO₂ has also been widely studied as both a support and promoter of Ni-based catalysts because of its high thermal stability, mechanical resistance, and high oxygen storage capacity. Dan et al. studied SMR over an Al₂O₃ supported Ni catalyst, which was previously modified with CeO₂ and La₂O₃. They observed that the morphological characteristics (i.e., surface

area, nickel dispersion) are responsible for the enhanced catalytic properties including larger methane conversion and a further decrease of coke formation [31]. As a summary, CeO_2 , ZrO_2 , and their mixed oxides are largely used as supports or support dopants, owing to their high oxygen storage capacity, redox properties, and consequently sufficient resistance to coking, leading to superior catalytic performance compared to conventional Al_2O_3 or MgAl_2O_4 supports [23].

2.5. Ni Coordination State

NiAl_2O_4 in the reduced and unreduced state, as well as NiAl_4O_7 in the reduced state, are active and stable for methane dry reforming due to the presence of 4-fold coordinated oxidized nickel. The limited amount of metallic nickel in these samples minimizes carbon deposition. On the other hand, the presence of metallic nickel is required for methane steam reforming (Figure 3). $\text{Ni}_2\text{Al}_2\text{O}_5$ in the reduced and unreduced states and NiAl_2O_4 in the reduced state are found to be active for methane steam reforming due to the presence of sufficiently small nickel nanoparticles that catalyze the reaction without accumulating carbonaceous deposits [32].

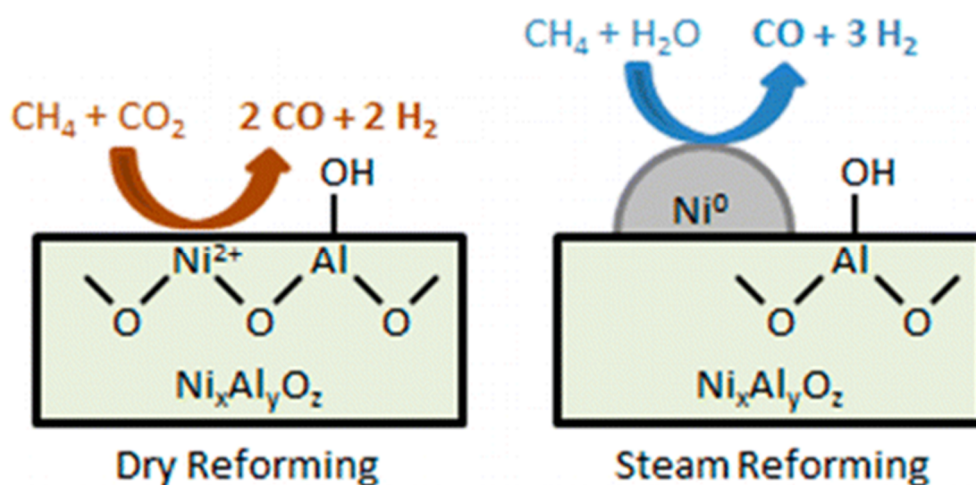


Figure 3. Active sites for methane dry reforming and methane steam reforming over nickel aluminate catalysts [32].

2.6. Catalyst Acidic/Basic Sites

The typical Al_2O_3 support for steam reforming catalysts is acidic and favors cracking and polymerization of hydrocarbons, which is the major reason to accelerate the deactivation of SMR catalysts. Alkali metals such as K and alkaline earth metals such as Mg and Ca are frequently used to improve catalyst stability [33]. Besides using promoters to modify Al_2O_3 support, researchers are seeking for alternative supports. Basic supports such as MgO and CaO could also prompt the reaction rate and H_2 selectivity via the enhanced sorption effect. Once these supports absorb CO_2 , the reaction equilibrium is shifted towards to the product side. Based on this effect, an SE-SMR process was developed to pursue higher H_2 selectivity [19–21]. Another advantage of the SE-SMR process is the ease of handling absorbed CO_2 by decomposing CaCO_3 and recovering the catalyst. However, regeneration of CaO is an exothermal reaction.

3. Descriptors of Reaction Kinetics

3.1. Surface Area of Ni Catalyst

Kinetic parameters are largely influenced by the catalysts and operation conditions. It was assumed that reactant species of CH_4 and CO_2 were adsorbed onto active sites separately. The adsorbed reactants then associatively react on the active sites and lead to the formation of H_2 and CO products. The basic

model is established on the basis that the reactant species of CH₄ and CO₂ follow the first-order behavior. Therefore, the optimization of reaction conditions and increasing surface area of Ni particles are the key for this aspect.

3.2. Binding Energy of Ni–C and Ni–O

The activation of CH₄ and the gasification of C species (to CO) are the rate-determined steps for SMR. Especially for the gasification of C species, the stronger bonding of Ni–C will hinder the desorption of C species and generate more carbon deposits (accelerate the deactivation). Previous research work [34] indicates that C or C–H species are the most stable intermediates on the catalyst surfaces. For the reverse reaction (i.e., methanation), the dissociation of CO has a large activation barrier on the perfect Ni(111) surface but is favored on the stepped Ni(211) surface. Hence, the steps on the Ni(111) surface are predicted to be the sites where CO dissociates. The reaction energy, 292 kJ/mol calculated from this DFT study, corresponds to a reaction enthalpy of 230 kJ/mol, which is in good agreement with the experimental value of 206 kJ/mol. The binding energy of Ni–C and Ni–O usually have a volcano-curve, therefore it is important to develop a Ni catalyst with optimized binding energy.

4. Descriptors of Reaction Engineering

The steps involved in the SMR process to produce pure H₂ can be divided into (a) feed pretreatment, (b) steam reforming, (c) CO shift conversion, and (d) hydrogen purification.

4.1. Temperature (Heat Transfer) and Pressure

SMR is severely endothermic ($\Delta H_{298K} = +205.9$ kJ/mol), and thus thermodynamically preferable under high temperature and low pressure. It has been demonstrated that ΔH of SMR increases as reaction temperature increases while ΔG reduces with the increasing temperature. In addition, low reaction temperature leads to coke deposition. Therefore, the SRM process usually runs at a higher temperature (above 700 °C) in order to maintain sufficient reaction activity [1]. For this endothermic reaction, the heat transfer is critical to keep the high reaction rate. Usually, Ni/Al₂O₃ powder was further coated on the commercial catalyst support. Hence, material type, shape and coating method all have great influence on the heat conductivity. At same time, the size of the used support is also important for saving the space of the reaction bed. The methane activation is one of the rate determined steps while the coverage of CH₄ on the Ni catalyst is crucial. Thus, the reaction should be carried out at a high pressure. On the other hand, due to the increased net number of product molecules, raising the reaction pressure will lower the methane conversion.

4.2. Ratio of H₂O/CH₄ in Feedstock

The conversion of methane depends on the steam to methane ratio (S/C), which increases with a higher S/C ratio, which varies from 1 to 5. Although the stoichiometry for SMR reactions suggests only 1 mol of H₂O is required for 1 mol of CH₄, the reaction in practice is being performed using high a S/C ratio, typically in the range 2.5–3 in order to reduce the risk of carbon deposition on the catalyst surface. At same time, a higher steam ratio will trigger more WGS reaction and change the H₂ selectivity. Herein, we listed the several commercial hydrogen production processes from methane in the below table, with the calculated CO₂/H₂ ratio. Theoretically, SMR produces one CO₂ together with four H₂ molecules (5.5 kg CO₂/kgH₂). For other processes yielding CO as by-product, researchers also consider further converting CO to CO₂ using a WGS reaction, and thus calculated the produced CO₂ amount, with polyoxometalate (POM) producing the highest amount of CO₂ while direct decomposition of methane to solid carbon and hydrogen undergoes a CO₂-free pathway (Table 1).

Table 1. Summary of different methane conversion processes.

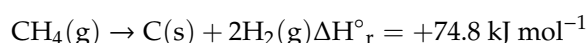
Reaction	Equation	ΔH_{298K} (kJ/mol)	Energy Input/mol _{H2}	Reaction Condition	Commercial Catalyst	CO ₂ /H ₂ (kg/kg)
SMR	$CH_4 + H_2O \leftrightarrow CO + 3H_2$	206	68	700–1000 °C	Ni/Al ₂ O ₃ (with promoter)	-
	$CH_4 + 2H_2O \leftrightarrow CO_2 + 4H_2$	165	41.2	3–25 bar		5.5
WGS	$CO + H_2O \leftrightarrow CO_2 + H_2$	-41	-41	HTS ¹	74.2% Fe ₂ O ₃	-
				310–450 °C	10.0% Cr ₂ O ₃	-
DRM	$CH_4 + CO_2 \leftrightarrow 2CO + 2H_2$	247	123.5	LTS ²	0.2% MgO	-
				200–250 °C	32–33% CuO	-
POM	$CH_4 + \frac{1}{2}O_2 \leftrightarrow CO + 2H_2$	-36	-18	800–1000 °C	34–53% ZnO	-
				10–20 bar	15–33% Al ₂ O ₃	5.5
Autothermal Reforming	$CH_4 + \frac{1}{3}O_2 + \frac{1}{3}H_2O \leftrightarrow C + \frac{7}{3}H_2$	46	20	400–1000 °C	Ni or Co-Based	5.5
				1 atm	Ni or Rh-based	7.3
Methane Decomposition	$CH_4 \leftrightarrow C(s) + 2H_2$	75	37.5	1500 °C	No catalyst	-
Hydrogen combustion	$H_2 + \frac{1}{2}O_2 \leftrightarrow H_2O$	-286	-	125 bar	-	6.6
Methane combustion	$CH_4 + 2O_2 \leftrightarrow CO_2 + 2H_2O$	-803	-	-	-	N.A.

¹ HTS: High Temperature Shift. ² LTS: Low Temperature Shift.

We also calculated the energy input (based on enthalpy) for generating one mole of H₂. Comparing with the energy output from the combustion of H₂ (−286 kJ/mol), all the processes have a net energy output, with POM having the largest amount of released energy, followed by autothermal reforming and then direct decomposition of methane. Therefore, when considering both the amount of released energy and produced CO₂, catalytic decomposition of methane to solid carbon is a promising and attractive alternative route for hydrogen production, especially due to its CO₂-free feature.

5. Catalytic Decomposition of Methane (CDM)

Methane can be directly thermally or thermocatalytically decomposed to carbon and hydrogen without emission CO₂ or CO, according to the following reaction:



Compared to other traditional hydrogen production from methane based on SMR and methane partial oxidation, which always generates large quantities of CO₂, the CDM process has recently attracted the most attention from researchers as it is the most environmentally friendly process for hydrogen [52–55]. For the CDM process, the suitable catalysts play a crucial role which can reduce the activation energy and shorten the reaction time. Typical catalysts include Ni based, Fe-based, doped noble metals and carbon catalysts [56–59].

Among all the CDM catalysts, Ni-based catalysts were widely investigated due to their high activity [60–62]. It has been reported that hydrogen could already be detected at 200 °C in the presence of a freshly prepared Ni catalyst [63]. Monzón and co-workers reported the results of the properties and catalytic behavior of an Al₂O₃ supported Ni catalyst with the loading amount of 30% (30% Ni/Al₂O₃) for CDM. The influence of operating and reduction temperatures and the composition of feeding gas (CH₄/H₂/N₂) on methane conversion, hydrogen production and deactivation of catalysts were further investigated. The result showed that the catalyst prepared by co-precipitation performs catalytic activity of methane decomposition reaction above 550 °C. Moreover, the feeding of hydrogen accompanied by methane inhibited both the formation of carbon filaments and coking reaction, which enhances the stability of catalysts to a certain degree [64].

The size of Ni particles plays a critical role in the reaction efficiency of CDM. Takenake et al., studied 40 wt% Ni/SiO₂ catalysts with 60–100 nm Ni nanoparticles in CDM, of which the carbon yield was as high as 491 g carbon per gram Ni at 500 °C [65]. As a comparison, Ermakove group prepared a 90 wt% Ni/SiO₂ catalyst with Ni particles of 10–40 nm size, which provided 385 g_C g_{Ni}^{−1} at 550 °C [66]. Modification of Ni catalysts with other metals to form bimetallic/trimetallic catalysts is another approach to increase the CDM activity and the stability of Ni catalysts [67,68]. Rezaei, Meshkani and co-workers investigated the catalytic and structural properties of the La, Ce, Co, Fe and Cu-promoted Ni/MgO·Al₂O₃ catalysts for thermal decomposition of methane. Compared to other elements, the addition of Cu to Ni/MgO·Al₂O₃ dramatically improved catalytic performance with the highest CH₄ conversion and H₂ yields due to the high activity of the NiCu alloy and fast diffusion of carbon. The results also demonstrated that the Ni–Cu/MgO·Al₂O₃ catalyst with 15 wt% Cu showed the highest catalytic activity and stability at higher temperature (>80% CH₄ conversion) [69]. Moreover, the methane decomposition activities of rare earth metals (La, Pr, Nd, Gd and Sm) doped Ni–Al catalysts were also explored. The introduction of rare earth elements into Ni/Al₂O₃ lead to the formation of a hydroxalite-like structure which greatly changed the activity of Ni particles. Among them, the Ni/Re/Al₂O₃ catalysts present best methane conversion due to the large surface area of Ni particles and the strong interaction between Ni and Re/Al₂O₃ [70].

Besides Ni catalysts, Fe-based catalysts are regarded as a promising material for CDM due to their high catalytic efficiency and environmentally friendly features. Furthermore, the partially filled 3d orbitals of Fe can promote the dissociation of hydrocarbon by slightly accepting electrons [71,72]. The Al_2O_3 and SiO_2 supported Fe catalysts were widely employed in the CDM reaction. Ibrahim and co-workers explored CH_4 conversion and H_2 yield of CDM at 700 °C over $\text{Fe}/\text{Al}_2\text{O}_3$ catalysts with different Fe loading amounts (14%–63%). The results indicated that at low Fe loading amounts, the yield of H_2 increased accompanying the content of Fe increase, which reached maximum of 77.2% with 42 wt% Fe loading amount. However, further increasing the Fe content lowered the hydrogen yield, resulting from reduced catalyst surface area caused by high Fe loading [73]. Similarly, Zhou et al. investigated the catalytic performance of $\text{Fe}/\text{Al}_2\text{O}_3$ with variable loading from 3.5 to 70 for CDM at 750 °C. At the loading amount of 41 wt%, the interaction of Fe_2O_3 and Al_2O_3 was the strongest, leading to an easy lattice incorporation-like solid solution. Therefore, the 41 wt% $\text{Fe}/\text{Al}_2\text{O}_3$ exhibited the best catalytic activity and stability with 80% methane conversion for 10 h at a reaction temperature of 750 °C. [74] On the other hand, SiO_2 is another common support which stabilizes Fe catalysts. Compared to $\text{Fe}/\text{Al}_2\text{O}_3$, Fe/SiO_2 always exhibited lower activity but longer lifetime due to the strong interaction between active Fe species and SiO_2 supports [75]. The Takenaka group compared the catalytic activity of $\text{Fe}/\text{Al}_2\text{O}_3$ and Fe/SiO_2 catalysts and found that the carbon yield of $\text{Fe}/\text{Al}_2\text{O}_3$ (22.5 gC gFe^{-1}) was higher than that of Fe/SiO_2 (7.5 gC gFe^{-1}) under the identical reaction condition, which results from the different catalytically active sites (α -Fe metal and Fe_3C) locally formed during the reaction (Figure 4). For $\text{Fe}/\text{Al}_2\text{O}_3$ with a smaller Fe particle size, Fe_2O_3 particles were converted to Fe_3C , while Fe_2O_3 over SiO_2 with a larger size always converted to α -Fe metallic species [76].

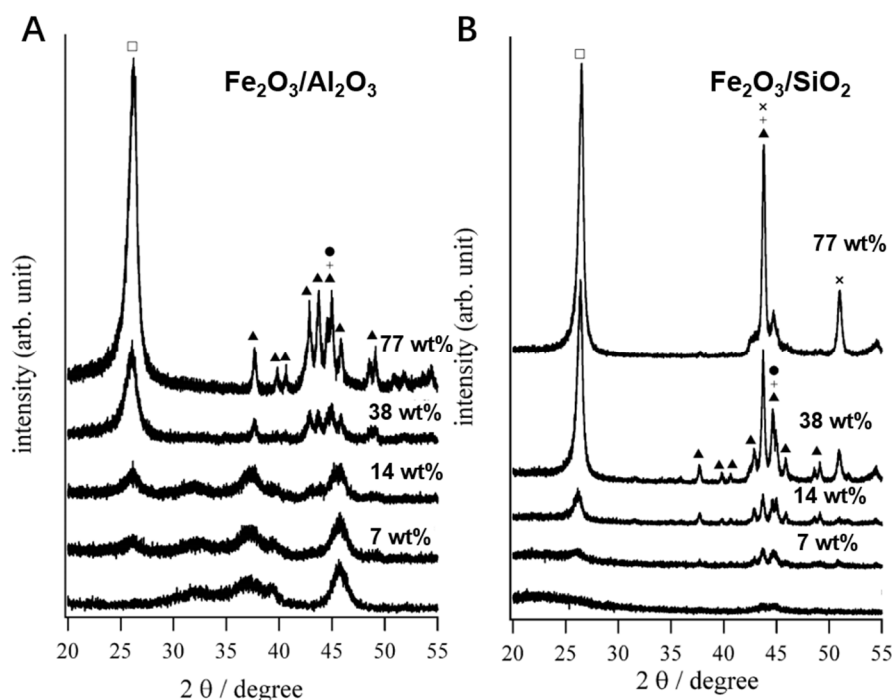


Figure 4. X-ray powder diffraction (XRD) patterns of (A) $\text{Fe}_2\text{O}_3/\text{Al}_2\text{O}_3$ and (B) $\text{Fe}_2\text{O}_3/\text{SiO}_2$ catalysts deactivated for catalytic decomposition of methane (CDM) at 1073 K. α -Fe metal (\bullet), Fe_3C (\blacktriangle) γ -Fe saturated with carbons (\times) and graphite (\square) [76].

Moreover, supported Fe-based bimetallic catalysts are employed in CDM as well, which always exhibited higher activity and stability than monometallic catalysts [77,78]. Pinilla et al. introduced Mo into Fe/MgO catalysts. The interaction between Mo and Fe particles could inhibit the agglomeration of Fe particles under the operation temperature. Therefore, the Fe/Mo/MgO exhibited good activity and stability in CDM with 87% methane conversion at 900 °C [79]. The Al-Fatesh group investigated a series of Fe/Ni/MgO catalysts with different ratios of Fe and Ni in CDM, among them the 15Fe/3Ni/MgO displayed the best catalytic property with 73% methane conversion at 700 °C, which was attributed to the presence of a suitable amount of non-interacted NiO species. With the increase in Ni content, CDM activity decreased due to the larger Ni particle size, lower metal dispersion, and thus the lower amount of active sites [80].

With the excellent capability to break up C–H bond, noble metal catalysts were also employed in CDM [81,82]. For instant, Takenaka, Otsuka and co-workers explored the effect of adding different noble metals (Rh, Pd, Ir and Pt) into supported Ni catalysts on the catalytic performance of methane decomposition. Compared to other added elements, the addition of Pd into Ni catalysts significantly improved the catalytic life time and hydrogen yield from CDM, which reached up to 390 gH₂ g(Pd+Ni)⁻¹ over the catalyst with, a mole ratio Pd/Ni of 1 with the total metal loading of 37 wt% on a carbon nanofiber support. Further experiments explained that the enhancement of activity and stability results from the formation of a Pd–Ni alloy. On the other hand, the pure Ni catalysts will deactivate due to the generation of nickel carbides, while Pd metal particles will fragment into smaller ones during the reaction on Pd catalysts. [83,84] Meanwhile, the Pudukudy group investigated the catalytic performance of Ni/SBA-15 promoted with different Pd loading. The addition of Pd allowed better dispersion of NiO on the support as well as reducing the reduction temperature of NiO due to the hydrogen spillover. Therefore, a maximum hydrogen yield of 59% was observed over the 0.4% Pd catalyst within 30 min, and there was no deactivation observed until 420 min under reaction conditions [85].

Although the CDM has been widely explored with a variety of different catalysts, there are still some challenges that limit its commercial application, especially the rapid deactivation by the produced carbon (coking reaction). In order to avoid the catalyst deactivation, the molten-metal catalyst was proposed by some researchers. Pure molten magnesium (Mg) was applied for CH₄ pyrolysis, which achieved 30% of the equilibrium conversion at 700 °C. However, the evaporation of Mg limited its higher conversion at a higher temperature [86]. Metiu, McFarland and co-workers dissolved an active metal (Ni) into an inactive low-melting temperature metal (Bi) to produce stable molten metal alloy catalysts for decomposition of methane to hydrogen and carbon (Figure 5). With the atomic partial negative Ni within the melt, the 27% Ni–73% Bi alloy achieved 95% methane conversion at 1065 °C in a 1.1 m bubble column and produced pure hydrogen without CO₂ or other by-products. On the other hand, in the molten alloy system, the insoluble carbon floats to the surface where it can be skimmed off, leading to the high stability of the molten-metal catalyst [87]. Furthermore, they further found that the molten Cu–Bi exhibited better catalytic activity compared to Ni–Bi system, even though neither molten Cu nor molten Bi are good methane pyrolysis catalysts. Further theoretical simulation indicated that the electron-deficient bismuth sites promote the dissociation of methane, leaving the CH₃ group bonded to bismuth and H connected to Cu [88].

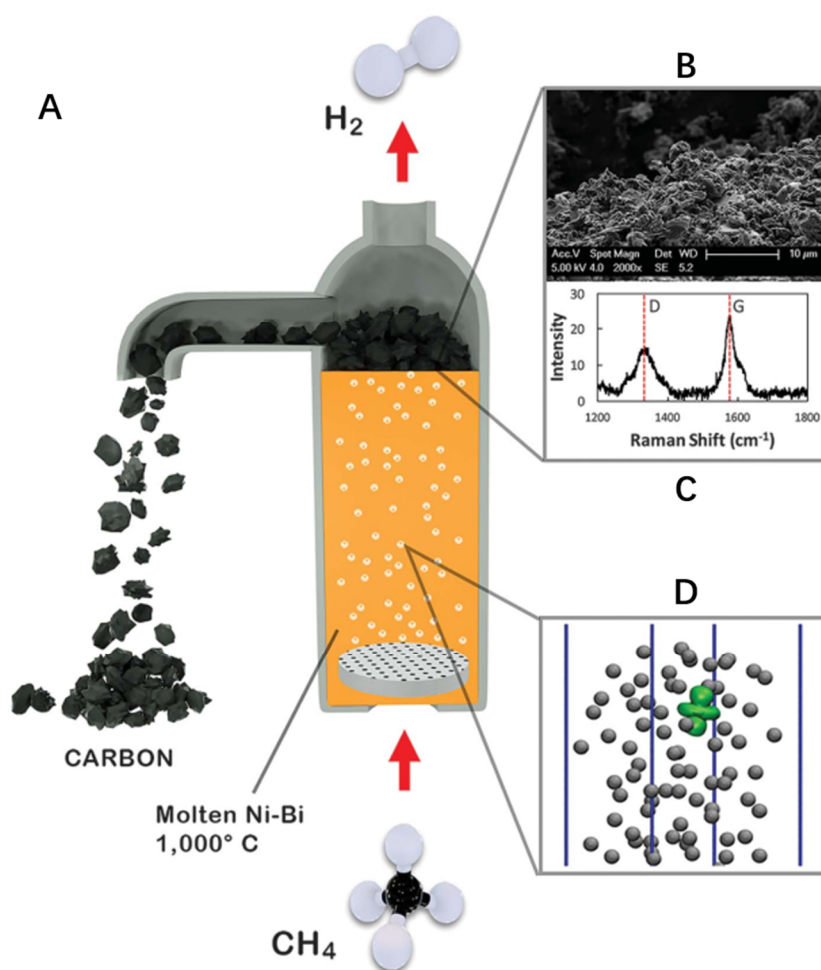


Figure 5. (A) Reactor for CDM over Ni–Bi molten alloy. (B) Scanning electron microscopy images and (C) Raman spectrum of produced carbon. (D) Ab initio molecular dynamics simulation showing an orbital (green) of a Pt atom dissolved in molten Bi (gray) [87].

6. Conversion of Methane to Other Hydrogen Containing Molecules

Compared to methane reforming processes which unavoidably release CO_x, or CDM process requiring high energy input, converting methane to other hydrogen-containing molecules (e.g., methanol, acetic acid) under a much milder condition followed by hydrogen generation, provides a new approach to utilize hydrogen from methane.

Selective oxidization of methane to methanol, which also contains four hydrogen atoms per molecule, is an efficient method to convert methane to a more active hydrogen-containing molecule. Moreover, as a liquid organic hydrogen carrier (LOHC) [89–91], methanol can release hydrogen by direct decomposition or methanol reforming [92,93]. The Hutchings group prepared a polyvinylpyrrolidone (PVP) stabilized Au–Pd alloy (Au:Pd = 1:1) and investigated its catalytic performance of CH₄ selective oxidation in H₂O₂ aqueous solution at 50 °C under 30 bar of CH₄. Compared to a TiO₂ supported Au–Pd alloy catalyst, the colloidal Au–Pd nanoparticles exhibited much better activity, with 92% selectivity at the mild temperature. An isotopical labeling experiment further indicated that most of the oxygenated products were formed from the gas-phase O₂ via a radical process, instead of H₂O₂ [94]. Xiao and co-workers reported a heterogenous catalytic system with high efficiency for selective oxidation methane to methanol with the in situ generated hydrogen peroxide at 70 °C (Figure 6). They encapsulated Au–Pd alloy particles into zeolite crystals and further modified the external surface of zeolite with organosilanes (AuPd@zeolite-R). The presence of silanes allowed the

diffusion of H_2 , O_2 and CH_4 to catalytic active sites while confining the generated H_2O_2 to increase the reaction probability. Therefore, AuPd@zeolite-R exhibited excellent performance with 17.3% methane conversion and 92% methanol selectivity [95]. Apart from common nanoparticle catalysts, certain particular methane monooxygenase (pMMO) is an enzyme catalyst for oxidation of methane to methanol in nature [96–98]. For example, extensive studies suggested that the active sites in pMMO are composed of copper complexes coordinated to histidine. Inspired by pMMO, our group employed MOF-808 as a scaffold to host and stabilize highly active copper–oxygen complexes. The catalyst showed high selectivity for methane oxidation to methanol under isothermal condition at 150 °C [99].

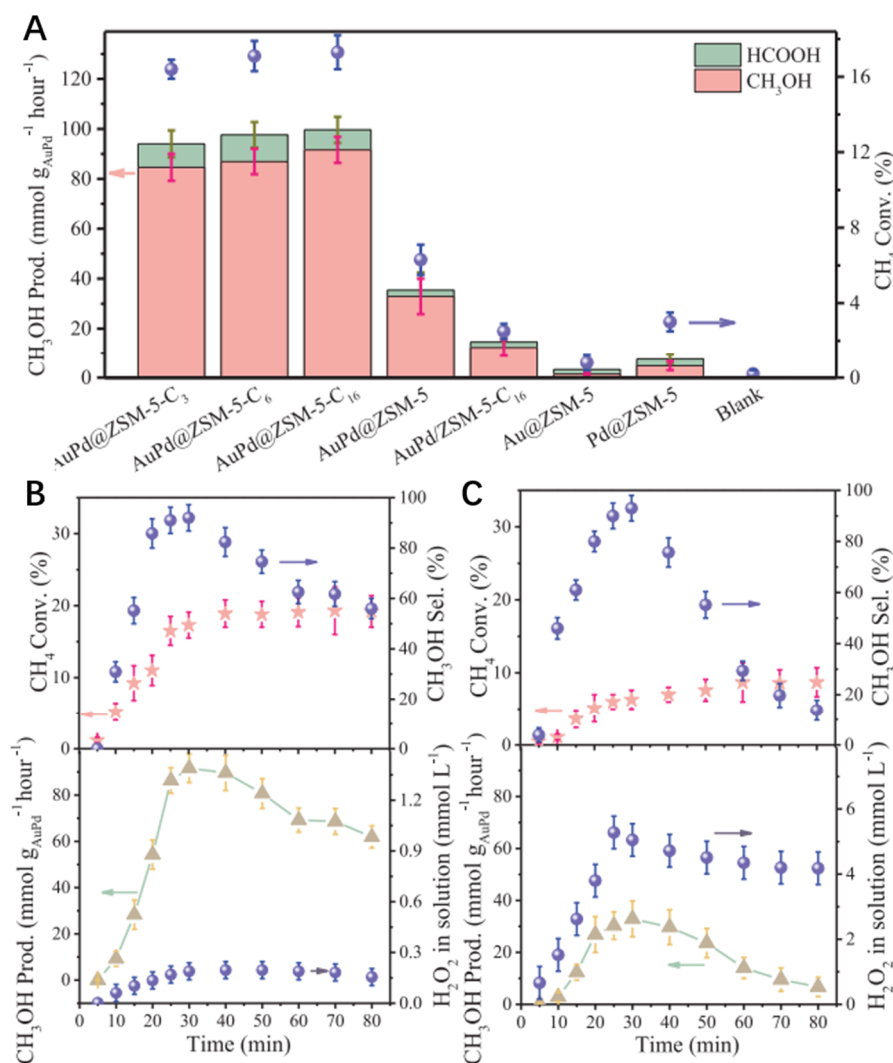


Figure 6. (A) CH_4 conversion and methanol selectivity over different catalysts. Dependences of the methane conversion (Conv.), methanol selectivity (Sel.), methanol productivity (Prod.), and H_2O_2 concentration in aqueous solution on reaction time over (B) AuPd@ZSM-5-C16 and (C) AuPd@ZSM-5 catalysts [95].

Besides methanol, methane could be directly transformed to acetic acid through oxidative carbonylation [100,101], which is regarded as another molecule for efficient hydrogen storage. The Flytzani-Stephanopoulos group employed mononuclear Rh species anchored on zeolite or TiO_2 catalysts for direct conversion of methane to methanol and acetic acid in aqueous solution in the presence of O_2 and CO at 150 °C. They found that for Rh-ZSM-5 catalysts, the yield of acetic acid was

around 22,000 $\mu\text{mol/g}_{\text{catalyst}}$ with more than 60% selectivity after a 3 h bath mode reaction, which was more efficient than direct conversion methane to methanol [102,103].

7. Conclusions

SMR still remains a complicated reaction process, which could be further optimized in terms of catalyst design and operational engineering. Nickel-based catalysts were widely studied due to their high activity and more importantly their low cost. Catalysts with better catalytic performance could be designed by following the descriptors mentioned in this review, including particle size effect, the selection of proper promoters and supports (e.g., CeO_2 and ZrO_2), and modification of coordination states. Moreover, reaction heat transfer, mass transfer, pressure drop, S/C ratio also need to be optimized for the industrial scale production. Unlike SMR and its derivative processes, which inevitably produce CO_2 as by-product, CDM benefits from its higher net energy output and CO_2 -free reaction pathway. The similar descriptors could be applied in the design of efficient catalysts for CDM as well. Particle size, addition of second metal, supports should all be taken into consideration to optimize the performance of catalysts. Notably, the use of molten metal catalysts provides an effective route for selective H_2 production from methane without catalyst deactivation via coke formation, which could be further explored in the future. Furthermore, more research interests were gained to convert methane to methanol as LOHC for easy and long-term hydrogen storage, providing a novel way to utilize methane for hydrogen economy.

Author Contributions: Conceptualization, J.S. and G.A.S.; Writing—original draft preparation, L.C., Z.Q., and S.Z.; Writing—review and editing, J.S.; Supervision, G.A.S. All authors have read and agreed to the published version of the manuscript.

Funding: The work shown in this paper was supported by Director, Office of Basic Energy Sciences, Division of Chemical Sciences, Geological and Biosciences of the U.S. Department of Energy under contract no. DE-AC02-05CH11231. This work was supported by the Hydrogen Materials Advanced Research Consortium (HyMARC), established as part of the Energy Materials Network by the U.S. Department of Energy, Office of Energy Efficiency and Renewable Energy, Fuel Cell Technologies Office, under Contract Number DE-AC02-05CH11231.

Conflicts of Interest: The authors declare no conflicts of interest.

References

1. Iulianelli, A.; Liguori, S.; Wilcox, J.; Basile, A. Advances on methane steam reforming to produce hydrogen through membrane reactors technology: A review. *Catal. Rev.* **2016**, *58*, 1–35. [[CrossRef](#)]
2. Barelli, L.; Bidini, G.; Gallorini, F.; Servili, S. Hydrogen production through sorption-enhanced steam methane reforming and membrane technology: A review. *Energy* **2008**, *33*, 554–570. [[CrossRef](#)]
3. Simpson, A.P.; Lutz, A.E. Exergy analysis of hydrogen production via steam methane reforming. *Int. J. Hydrogen Energy* **2007**, *32*, 4811–4820. [[CrossRef](#)]
4. LeValley, T.L.; Richard, A.R.; Fan, M. The progress in water gas shift and steam reforming hydrogen production technologies—A review. *Int. J. Hydrogen Energy* **2014**, *39*, 16983–17000. [[CrossRef](#)]
5. Parthasarathy, P.; Narayanan, K.S. Hydrogen production from steam gasification of biomass: Influence of process parameters on hydrogen yield—A review. *Renew. Energy* **2014**, *66*, 570–579. [[CrossRef](#)]
6. Zhang, L.; Roling, L.T.; Wang, X.; Vara, M.; Chi, M.; Liu, J.; Choi, S.I.; Park, J.; Herron, J.A.; Xie, Z.; et al. Platinum-based nanocages with subnanometer-thick walls and well-defined, controllable facets. *Science* **2015**, *349*, 412–416. [[CrossRef](#)]
7. Chen, L.N.; Li, H.Q.; Yan, M.W.; Yuan, C.F.; Zhan, W.W.; Jiang, Y.Q.; Xie, Z.X.; Kuang, Q.; Zheng, L.S. Ternary Alloys Encapsulated within Different MOFs via a Self-Sacrificing Template Process: A Potential Platform for the Investigation of Size-Selective Catalytic Performances. *Small* **2017**, *13*, 1700683. [[CrossRef](#)]
8. Qiao, B.; Wang, A.; Yang, X.; Allard, L.F.; Jiang, Z.; Cui, Y.; Liu, J.; Li, J.; Zhang, T. Single-atom catalysis of CO oxidation using Pt_1/FeO_x . *Nat. Chem.* **2011**, *3*, 634–641. [[CrossRef](#)]
9. Sun, P.; Young, B.; Elgowainy, A.; Lu, Z.; Wang, M.; Morelli, B.; Hawkins, T. Criteria Air Pollutants and Greenhouse Gas Emissions from Hydrogen Production in US Steam Methane Reforming Facilities. *Environ. Sci. Technol.* **2019**, *53*, 7103–7113. [[CrossRef](#)]

10. Pakhare, D.; Spivey, J. A review of dry (CO₂) reforming of methane over noble metal catalysts. *Chem. Soc. Rev.* **2014**, *43*, 7813–7837. [[CrossRef](#)]
11. Lavoie, J.M. Review on dry reforming of methane, a potentially more environmentally-friendly approach to the increasing natural gas exploitation. *Front. Chem.* **2014**, *2*, 1–17. [[CrossRef](#)] [[PubMed](#)]
12. Wang, Y.; Yao, L.; Wang, Y.; Wang, S.; Zhao, Q.; Mao, D.; Hu, C. Low-temperature catalytic CO₂ dry reforming of methane on Ni-Si/ZrO₂ catalyst. *ACS Catal.* **2018**, *8*, 6495–6506. [[CrossRef](#)]
13. Enger, B.C.; Lødeng, R.; Holmen, A. A review of catalytic partial oxidation of methane to synthesis gas with emphasis on reaction mechanisms over transition metal catalysts. *Appl. Catal. A* **2018**, *346*, 1–27. [[CrossRef](#)]
14. Choudhary, V.R.; Mondal, K.C.; Choudhary, T.V. Partial oxidation of methane to syngas with or without simultaneous steam or CO₂ reforming over a high-temperature stable-NiCoMgCeO_x supported on zirconia-hafnia catalyst. *Appl. Catal. A* **2016**, *306*, 45–50. [[CrossRef](#)]
15. Jabbour, K. Tuning combined steam and dry reforming of methane for “metgas” production: A thermodynamic approach and state-of-the-art catalysts. *J. Energy Chem.* **2000**, *48*, 54–91. [[CrossRef](#)]
16. Angeli, S.D.; Turchetti, L.; Monteleone, G.; Lemonidou, A.A. Catalyst development for steam reforming of methane and model biogas at low temperature. *Appl. Catal. B* **2016**, *181*, 34–46. [[CrossRef](#)]
17. Chen, L.; Gangadharan, P.; Lou, H.H. Sustainability assessment of combined steam and dry reforming versus tri-reforming of methane for syngas production. *Asia-Pac. J. Chem. Eng.* **2018**, *13*, 1–13. [[CrossRef](#)]
18. Zhao, K.; He, F.; Huang, Z.; Wei, G.; Zheng, A.; Li, H.; Zhao, Z. Perovskite-type oxides LaFe_{1-x}Co_xO₃ for chemical looping steam methane reforming to syngas and hydrogen co-production. *Appl. Energy* **2016**, *168*, 193–203. [[CrossRef](#)]
19. Zhao, C.; Zhou, Z.; Cheng, Z.; Fang, X. Sol-gel-derived, CaZrO₃-stabilized Ni/CaO-CaZrO₃ bifunctional catalyst for sorption-enhanced steam methane reforming. *Appl. Catal. B* **2016**, *196*, 16–26. [[CrossRef](#)]
20. Dou, B.; Wang, C.; Song, Y.; Chen, H.; Jiang, B.; Yang, M.; Xu, Y. Solid sorbents for in-situ CO₂ removal during sorption-enhanced steam reforming process: A review. *Renew. Sustain. Energy Rev.* **2016**, *53*, 536–546. [[CrossRef](#)]
21. Harrison, D.P. Sorption-enhanced hydrogen production: A review. *Ind. Eng. Chem. Res.* **2008**, *47*, 6486–6501. [[CrossRef](#)]
22. Papalás, T.; Antzarás, A.N.; Lemonidou, A.A. Intensified steam methane reforming coupled with Ca-Ni looping in a dual fluidized bed reactor system: A conceptual design. *Chem. Eng. J.* **2020**, *382*, 122993. [[CrossRef](#)]
23. Meloni, E.; Martino, M.; Palma, V. A Short Review on Ni Based Catalysts and Related Engineering Issues for Methane Steam Reforming. *Catalysts* **2020**, *10*, 352. [[CrossRef](#)]
24. Vogt, C.; Kranenborg, J.; Monai, M.; Weckhuysen, B.M. Structure sensitivity in steam and dry methane reforming over nickel: Activity and carbon formation. *ACS Catal.* **2019**, *10*, 1428–1438. [[CrossRef](#)]
25. Jones, G.; Jakobsen, J.G.; Shim, S.S.; Kleis, J.; Andersson, M.P.; Rossmesl, J.; Abild-Pedersen, F.; Bligaard, T.; Helveg, S.; Hinnemann, B.; et al. First principles calculations and experimental insight into methane steam reforming over transition metal catalysts. *J. Catal.* **2008**, *259*, 147–160. [[CrossRef](#)]
26. Wei, J.; Iglesia, E. Isotopic and kinetic assessment of the mechanism of reactions of CH₄ with CO₂ or H₂O to form synthesis gas and carbon on nickel catalysts. *J. Catal.* **2004**, *224*, 370–383. [[CrossRef](#)]
27. Zuo, Z.; Liu, S.; Wang, Z.; Liu, C.; Huang, W.; Huang, J.; Liu, P. Dry reforming of methane on single-site Ni/MgO catalysts: Importance of site confinement. *ACS Catal.* **2018**, *8*, 9821–9835. [[CrossRef](#)]
28. Huang, J.; Liu, W.; Yang, Y.; Liu, B. High-performance Ni-Fe redox catalysts for selective CH₄ to syngas conversion via chemical looping. *ACS Catal.* **2018**, *8*, 1748–1756. [[CrossRef](#)]
29. Nieva, M.A.; Villaverde, M.M.; Monzón, A.; Garetto, T.F.; Marchi, A.J. Steam-methane reforming at low temperature on nickel-based catalysts. *Chem. Eng. J.* **2014**, *235*, 158–166. [[CrossRef](#)]
30. Matsumura, Y.; Nakamori, T. Steam reforming of methane over nickel catalysts at low reaction temperature. *Appl. Catal. A* **2004**, *258*, 107–114. [[CrossRef](#)]
31. Chihaiá, V.; Sohlberg, K.; Dan, M.; Mihet, M.; Biris, A.R.; Marginean, P.; Almasan, V.; Borodi, G.; Watanabe, F.; Biris, A.S.; et al. Supported nickel catalysts for low temperature methane steam reforming: Comparison between metal additives and support modification. *React. Kinet. Mech. Catal.* **2012**, *105*, 173–193.
32. Rogers, J.L.; Mangarella, M.C.; D’Amico, A.D.; Gallagher, J.R.; Dutzer, M.R.; Stavitski, E.; Miller, J.T.; Sievers, C. Differences in the nature of active sites for methane dry reforming and methane steam reforming over nickel aluminate catalysts. *ACS Catal.* **2016**, *6*, 5873–5886. [[CrossRef](#)]

33. Lisboa, J.D.S.; Santos, D.C.; Passos, F.B.; Noronha, F.B. Influence of the addition of promoters to steam reforming catalysts. *Catal. Today* **2005**, *101*, 15–21. [[CrossRef](#)]
34. Li, X.; Li, D.; Tian, H.; Zeng, L.; Zhao, Z.J.; Gong, J. Dry reforming of methane over Ni/La₂O₃ nanorod catalysts with stabilized Ni nanoparticles. *Appl. Catal. B.* **2017**, *202*, 683–694. [[CrossRef](#)]
35. Aramouni, N.A.K.; Touma, J.G.; Tarboush, B.A.; Zeaiter, J.; Ahmad, M.N. Catalyst design for dry reforming of methane: Analysis review. *Renew. Sustain. Energ. Rev.* **2018**, *82*, 2570–2585. [[CrossRef](#)]
36. Usman, M.; Daud, W.W.; Abbas, H.F. Dry reforming of methane: Influence of process parameters-A review. *Renew. Sustain. Energ. Rev.* **2015**, *45*, 710–744. [[CrossRef](#)]
37. Song, Y.; Ozdemir, E.; Ramesh, S.; Adishev, A.; Subramanian, S.; Harale, A.; Albuali, M.; Fadhel, B.A.; Jamal, A.; Moon, D.; et al. Dry reforming of methane by stable Ni-Mo nanocatalysts on single-crystalline MgO. *Science* **2020**, *367*, 777–781. [[CrossRef](#)]
38. Zhou, L.; Martirez, J.M.P.; Finzel, J.; Zhang, C.; Swearer, D.F.; Tian, S.; Robotjazi, H.; Lou, M.; Dong, L.; Henderson, L.; et al. Light-driven methane dry reforming with single atomic site antenna-reactor plasmonic photocatalysts. *Nat. Energy* **2020**, *5*, 61–70. [[CrossRef](#)]
39. Tang, Y.; Wei, Y.; Wang, Z.; Zhang, S.; Li, Y.; Nguyen, L.; Li, Y.; Zhou, Y.; Shen, W.; Tao, F.F.; et al. Synergy of single-atom Ni₁ and Ru₁ sites on CeO₂ for dry reforming of CH₄. *J. Am. Chem. Soc.* **2019**, *141*, 7283–7293. [[CrossRef](#)]
40. Theofanidis, S.A.; Galvita, V.V.; Poelman, H.; Marin, G.B. Enhanced carbon-resistant dry reforming Fe-Ni catalyst: Role of Fe. *ACS Catal.* **2015**, *5*, 3028–3039. [[CrossRef](#)]
41. Abelló, S.; Bolshak, E.; Montane, D. Ni-Fe catalysts derived from hydrotalcite-like precursors for hydrogen production by ethanol steam reforming. *Appl. Catal. A* **2013**, *450*, 261–274. [[CrossRef](#)]
42. Profeti, L.P.; Ticianelli, E.A.; Assaf, E.M. Co/Al₂O₃ catalysts promoted with noble metals for production of hydrogen by methane steam reforming. *Fuel* **2008**, *87*, 2076–2081. [[CrossRef](#)]
43. Akri, M.; Zhao, S.; Li, X.; Zang, K.; Lee, A.F.; Isaacs, M.A.; Xi, W.; Gangarajula, Y.; Luo, J.; Ren, Y.; et al. Atomically dispersed nickel as coke-resistant active sites for methane dry reforming. *Nat. Commun.* **2019**, *10*, 1–10. [[CrossRef](#)] [[PubMed](#)]
44. Maluf, S.S.; Assaf, E.M. Ni catalysts with Mo promoter for methane steam reforming. *Fuel* **2009**, *88*, 1547–1553. [[CrossRef](#)]
45. Nikolla, E.; Schwank, J.; Linic, S. Comparative study of the kinetics of methane steam reforming on supported Ni and Sn/Ni alloy catalysts: The impact of the formation of Ni alloy on chemistry. *J. Catal.* **2009**, *263*, 220–227. [[CrossRef](#)]
46. Wu, H.; La Parola, V.; Pantaleo, G.; Puleo, F.; Venezia, A.M.; Liotta, L.F. Ni-based catalysts for low temperature methane steam reforming: Recent results on Ni-Au and comparison with other bi-metallic systems. *Catalysts* **2013**, *3*, 563–583. [[CrossRef](#)]
47. Ay, H.; Üner, D. Dry reforming of methane over CeO₂ supported Ni, Co and Ni-Co catalysts. *Appl. Catal. B* **2015**, *179*, 128–138. [[CrossRef](#)]
48. Guo, J.; Lou, H.; Zhao, H.; Chai, D.; Zheng, X. Dry reforming of methane over nickel catalysts supported on magnesium aluminate spinels. *Appl. Catal. A* **2004**, *273*, 75–82. [[CrossRef](#)]
49. Laosiripojana, N.; Assabumrungrat, S. Methane steam reforming over Ni/Ce-ZrO₂ catalyst: Influences of Ce-ZrO₂ support on reactivity, resistance toward carbon formation, and intrinsic reaction kinetics. *Appl. Catal. A* **2005**, *290*, 200–211. [[CrossRef](#)]
50. Zhang, S.; Muratsugu, S.; Ishiguro, N.; Tada, M. Ceria-doped Ni/SBA-16 catalysts for dry reforming of methane. *ACS Catal.* **2013**, *3*, 1855–1864. [[CrossRef](#)]
51. Palmer, C.; Upham, D.C.; Smart, S.; Gordon, M.J.; Metiu, H.; McFarland, E.W. Dry reforming of methane catalysed by molten metal alloys. *Nat. Catal.* **2020**, *3*, 83–89. [[CrossRef](#)]
52. Choudhary, T.V.; Sivadinarayana, C.; Chusuei, C.C.; Klinghoffer, A.; Goodman, D.W. Hydrogen production via catalytic decomposition of methane. *J. Catal.* **2001**, *199*, 9–18. [[CrossRef](#)]
53. Muradov, N. Hydrogen via methane decomposition: An application for decarbonization of fossil fuels. *Int. J. Hydrogen Energy* **2001**, *26*, 1165–1175. [[CrossRef](#)]
54. Zhang, J.; Li, X.; Chen, H.; Qi, M.; Zhang, G.; Hu, H.; Ma, X. Hydrogen production by catalytic methane decomposition: Carbon materials as catalysts or catalyst supports. *Int. J. Hydrogen Energy* **2017**, *42*, 19755–19775. [[CrossRef](#)]

55. Qian, J.X.; Chen, T.W.; Enakonda, L.R.; Liu, D.B.; Mignani, G.; Basset, J.M.; Zhou, L. Methane decomposition to produce CO_x-free hydrogen and nano-carbon over metal catalysts: A review. *Int. J. Hydrogen Energy* **2020**, *45*, 7981–8001. [[CrossRef](#)]
56. Chen, D.; Christensen, K.O.; Ochoa-Fernández, E.; Yu, Z.; Tøtdal, B.; Latorre, N.; Monzón, A.; Holmen, A. Synthesis of carbon nanofibers: Effects of Ni crystal size during methane decomposition. *J. Catal.* **2005**, *229*, 82–96. [[CrossRef](#)]
57. Reshетенko, T.V.; Avdeeva, L.B.; Ismagilov, Z.R.; Chuvilin, A.L.; Ushakov, V.A. Carbon capacious Ni-Cu-Al₂O₃ catalysts for high-temperature methane decomposition. *Appl. Catal. A* **2003**, *247*, 51–63. [[CrossRef](#)]
58. Avdeeva, L.B.; Reshетенko, T.V.; Ismagilov, Z.R.; Likholobov, V.A. Iron-containing catalysts of methane decomposition: Accumulation of filamentous carbon. *Appl. Catal. A* **2002**, *228*, 53–63. [[CrossRef](#)]
59. Muradov, N. Catalysis of methane decomposition over elemental carbon. *Catal. Commun.* **2001**, *2*, 89–94. [[CrossRef](#)]
60. Takenaka, S.; Ogihara, H.; Yamanaka, I.; Otsuka, K. Decomposition of methane over supported-Ni catalysts: Effects of the supports on the catalytic lifetime. *Appl. Catal. A* **2001**, *217*, 101–110. [[CrossRef](#)]
61. Li, Y.; Zhang, B.; Tang, X.; Xu, Y.; Shen, W. Hydrogen production from methane decomposition over Ni/CeO₂ catalysts. *Catal. Commun.* **2006**, *7*, 380–386. [[CrossRef](#)]
62. Chen, L.; Zhang, X.; Zhou, J.; Xie, Z.; Kuang, Q.; Zheng, L. A nano-reactor based on PtNi@ metal-organic framework composites loaded with polyoxometalates for hydrogenation-esterification tandem reactions. *Nanoscale* **2019**, *11*, 3292–3299. [[CrossRef](#)] [[PubMed](#)]
63. Rostrup-Nielsen, J.R.; Sehested, J.; Nørskov, J.K. Hydrogen and synthesis gas by steam-and CO₂ reforming. *Adv. Catal.* **2002**, *47*, 65–139. [[CrossRef](#)]
64. Abbas, H.F.; Daud, W.W. Hydrogen production by methane decomposition: A review. *Int. J. Hydrogen Energy* **2010**, *35*, 1160–1190. [[CrossRef](#)]
65. Villacampa, J.I.; Royo, C.; Romeo, E.; Montoya, J.A.; Del Angel, P.; Monzon, A. Catalytic decomposition of methane over Ni-Al₂O₃ coprecipitated catalysts: Reaction and regeneration studies. *Appl. Catal. A* **2013**, *252*, 363–383. [[CrossRef](#)]
66. Takenaka, S.; Kobayashi, S.; Ogihara, H.; Otsuka, K. Ni/SiO₂ catalyst effective for methane decomposition into hydrogen and carbon nanofiber. *J. Catal.* **2013**, *217*, 79–87. [[CrossRef](#)]
67. Ermakova, M.A.; Ermakov, D.Y.; Kuvshinov, G.G.; Plyasova, L.M. New nickel catalysts for the formation of filamentous carbon in the reaction of methane decomposition. *J. Catal.* **1999**, *187*, 77–84. [[CrossRef](#)]
68. Chen, L.; Li, H.; Zhan, W.; Cao, Z.; Chen, J.; Jiang, Q.; Jiang, Y.; Xie, Z.; Kuang, Q.; Zheng, L. Controlled encapsulation of flower-like Rh-Ni alloys with MOFs via tunable template Dealloying for enhanced selective hydrogenation of alkyne. *ACS Appl. Mater. Interfaces* **2016**, *8*, 31059–31066. [[CrossRef](#)]
69. Rastegarpanah, A.; Meshkani, F.; Rezaei, M. Thermocatalytic decomposition of methane over mesoporous nanocrystalline promoted Ni/MgO-Al₂O₃ catalysts. *Int. J. Hydrogen Energy* **2017**, *42*, 16476–16488. [[CrossRef](#)]
70. Anjaneyulu, C.; Naresh, G.; Kumar, V.V.; Tardio, J.; Rao, T.V.; Venugopal, A. Influence of rare earth (La, Pr, Nd, Gd, and Sm) metals on the methane decomposition activity of Ni-Al catalysts. *ACS Sustain. Chem. Eng.* **2015**, *3*, 1298–1305. [[CrossRef](#)]
71. Zhou, L.; Enakonda, L.R.; Harb, M.; Saih, Y.; Aguilar-Tapia, A.; Ould-Chikh, S.; Hazemann, J.L.; Li, J.; Wei, N.; Gary, D.; et al. Fe catalysts for methane decomposition to produce hydrogen and carbon nano materials. *Appl. Catal. B* **2017**, *208*, 44–59. [[CrossRef](#)]
72. Jin, L.; Si, H.; Zhang, J.; Lin, P.; Hu, Z.; Qiu, B.; Hu, H. Preparation of activated carbon supported Fe-Al₂O₃ catalyst and its application for hydrogen production by catalytic methane decomposition. *Int. J. Hydrogen Energy* **2013**, *38*, 10373–10380. [[CrossRef](#)]
73. Ibrahim, A.A.; Fakeeha, A.H.; Al-Fatesh, A.S.; Abasaeed, A.E.; Khan, W.U. Methane decomposition over iron catalyst for hydrogen production. *Int. J. Hydrogen Energy* **2015**, *40*, 7593–7600. [[CrossRef](#)]
74. Zhou, L.; Enakonda, L.R.; Saih, Y.; Loptain, S.; Gary, D.; Del-Gallo, P.; Basset, J.M. Catalytic methane decomposition over Fe-Al₂O₃. *ChemSusChem* **2016**, *9*, 1243–1248. [[CrossRef](#)]
75. Ermakova, M.A.; Ermakov, D.Y. Ni/SiO₂ and Fe/SiO₂ catalysts for production of hydrogen and filamentous carbon via methane decomposition. *Catal. Today* **2002**, *77*, 225–235. [[CrossRef](#)]
76. Takenaka, S.; Serizawa, M.; Otsuka, K. Formation of filamentous carbons over supported Fe catalysts through methane decomposition. *J. Catal.* **2014**, *222*, 520–531. [[CrossRef](#)]

77. Hu, X.; Hu, Y.; Xu, Q.; Wang, X.; Li, G.; Cheng, H.; Zou, X.; Lu, X. Molten salt-promoted Ni-Fe/Al₂O₃ catalyst for methane decomposition. *Int. J. Hydrogen Energy* **2020**, *45*, 4244–4253. [[CrossRef](#)]
78. Tang, L.; Yamaguchi, D.; Burke, N.; Trimm, D.; Chiang, K. Methane decomposition over ceria modified iron catalysts. *Catal. Commun.* **2010**, *11*, 1215–1219. [[CrossRef](#)]
79. Pinilla, J.L.; Utrilla, R.; Karn, R.K.; Suelves, I.; Lázaro, M.J.; Moliner, R.; García, A.B.; Rouzaud, J.N. High temperature iron-based catalysts for hydrogen and nanostructured carbon production by methane decomposition. *Int. J. Hydrogen Energy* **2011**, *36*, 7832–7843. [[CrossRef](#)]
80. Al-Fatesh, A.S.; Barama, S.; Ibrahim, A.A.; Barama, A.; Khan, W.U.; Fakeeha, A. Study of methane decomposition on Fe/MgO-based catalyst modified by Ni, Co, and Mn additives. *Chem. Eng. Commun.* **2017**, *204*, 739–749. [[CrossRef](#)]
81. Salazar-Villalpando, M.D.; Miller, A.C. Hydrogen production by methane decomposition and catalytic partial oxidation of methane over Pt/Ce_xGd_{1-x}O₂ and Pt/Ce_xZr_{1-x}O₂. *Chem. Eng. J.* **2011**, *166*, 738–743. [[CrossRef](#)]
82. Persson, K.; Ersson, A.; Jansson, K.; Fierro, J.L.G.; Järås, S.G. Influence of molar ratio on Pd–Pt catalysts for methane combustion. *J. Catal.* **2006**, *243*, 14–24. [[CrossRef](#)]
83. Takenaka, S.; Shigeta, Y.; Tanabe, E.; Otsuka, K. Methane decomposition into hydrogen and carbon nanofibers over supported Pd–Ni catalysts. *J. Catal.* **2013**, *220*, 468–477. [[CrossRef](#)]
84. Takenaka, S.; Shigeta, Y.; Tanabe, E.; Otsuka, K. Methane decomposition into hydrogen and carbon nanofibers over supported Pd–Ni catalysts: Characterization of the catalysts during the reaction. *J. Phys. Chem. B* **2014**, *108*, 7656–7664. [[CrossRef](#)]
85. Pudukudy, M.; Yaakob, Z.; Akmal, Z.S. Direct decomposition of methane over Pd promoted Ni/SBA-15 catalysts. *Appl. Surf. Sci.* **2015**, *353*, 127–136. [[CrossRef](#)]
86. Wang, K.; Li, W.S.; Zhou, X.P. Hydrogen generation by direct decomposition of hydrocarbons over molten magnesium. *J. Mol. Catal. A Chem.* **2008**, *283*, 153–157. [[CrossRef](#)]
87. Upham, D.C.; Agarwal, V.; Khechfe, A.; Snodgrass, Z.R.; Gordon, M.J.; Metiu, H.; McFarland, E.W. Catalytic molten metals for the direct conversion of methane to hydrogen and separable carbon. *Science* **2017**, *358*, 917–921. [[CrossRef](#)]
88. Palmer, C.; Tarazkar, M.; Kristoffersen, H.H.; Gelinas, J.; Gordon, M.J.; McFarland, E.W.; Metiu, H. Methane pyrolysis with a molten Cu–Bi alloy catalyst. *ACS Catal.* **2019**, *9*, 8337–8345. [[CrossRef](#)]
89. Teichmann, D.; Arlt, W.; Wasserscheid, P.; Freymann, R. A future energy supply based on Liquid Organic Hydrogen Carriers (LOHC). *Energy Environ. Sci.* **2011**, *4*, 2767–2773. [[CrossRef](#)]
90. Preuster, P.; Papp, C.; Wasserscheid, P. Liquid organic hydrogen carriers (LOHCs): Toward a hydrogen-free hydrogen economy. *Acc. Chem. Res.* **2017**, *50*, 74–85. [[CrossRef](#)]
91. Teichmann, D.; Arlt, W.; Wasserscheid, P. Liquid Organic Hydrogen Carriers as an efficient vector for the transport and storage of renewable energy. *Int. J. Hydrogen Energy* **2012**, *37*, 18118–18132. [[CrossRef](#)]
92. Chen, L.N.; Hou, K.P.; Liu, Y.S.; Qi, Z.Y.; Zheng, Q.; Lu, Y.H.; Chen, J.Y.; Chen, J.L.; Pao, C.W.; Wang, S.B.; et al. Efficient hydrogen production from methanol using a single-site Pt₁/CeO₂ catalyst. *J. Am. Chem. Soc.* **2019**, *141*, 17995–17999. [[CrossRef](#)]
93. Lin, L.; Zhou, W.; Gao, R.; Yao, S.; Zhang, X.; Xu, W.; Zheng, S.; Jiang, Z.; Yu, Q.; Li, Y.W.; et al. Low-temperature hydrogen production from water and methanol using Pt/α-MoC catalysts. *Nature* **2017**, *544*, 80–83. [[CrossRef](#)]
94. Agarwal, N.; Freakley, S.J.; McVicker, R.U.; Althahban, S.M.; Dimitratos, N.; He, Q.; Morgan, D.J.; Jenkins, R.L.; Willock, D.J.; Taylor, S.H.; et al. Aqueous Au–Pd colloids catalyze selective CH₄ oxidation to CH₃OH with O₂ under mild conditions. *Science* **2017**, *358*, 223–227. [[CrossRef](#)]
95. Jin, Z.; Wang, L.; Zuidema, E.; Mondal, K.; Zhang, M.; Zhang, J.; Wang, C.; Meng, X.; Yang, H.; Mesters, C.; et al. Hydrophobic zeolite modification for in situ peroxide formation in methane oxidation to methanol. *Science* **2020**, *367*, 193–197.
96. Balasubramanian, R.; Smith, S.M.; Rawat, S.; Yatsunyk, L.A.; Stemmler, T.L.; Rosenzweig, A.C. Oxidation of methane by a biological dicopper centre. *Nature* **2010**, *465*, 115–119. [[CrossRef](#)]
97. Baik, M.H.; Newcomb, M.; Friesner, R.A.; Lippard, S.J. Mechanistic studies on the hydroxylation of methane by methane monooxygenase. *Chem. Rev.* **2003**, *103*, 2385–2420. [[CrossRef](#)]
98. Lipscomb, J.D. Biochemistry of the soluble methane monooxygenase. *Annu. Rev. Microbiol.* **1994**, *48*, 371–399. [[CrossRef](#)]

99. Baek, J.; Rungtaweivoranit, B.; Pei, X.; Park, M.; Fakra, S.C.; Liu, Y.S.; Matheu, R.; Alshimri, S.A.; Alshehri, S.; Trickett, C.A.; et al. Bioinspired Metal–Organic framework catalysts for selective methane oxidation to methanol. *J. Am. Chem. Soc.* **2018**, *140*, 18208–18216. [[CrossRef](#)]
100. Lin, M.; Sen, A. Direct catalytic conversion of methane to acetic acid in an aqueous medium. *Nature* **1994**, *368*, 613–615. [[CrossRef](#)]
101. Kwon, Y.; Kim, T.Y.; Kwon, G.; Yi, J.; Lee, H. Selective activation of methane on single-atom catalyst of rhodium dispersed on zirconia for direct conversion. *J. Am. Chem. Soc.* **2017**, *139*, 17694–17699. [[CrossRef](#)]
102. Shan, J.; Li, M.; Allard, L.F.; Lee, S.; Flytzani-Stephanopoulos, M. Mild oxidation of methane to methanol or acetic acid on supported isolated rhodium catalysts. *Nature* **2017**, *551*, 605–608. [[CrossRef](#)]
103. Tang, Y.; Li, Y.; Fung, V.; Jiang, D.E.; Huang, W.; Zhang, S.; Iwasawa, Y.; Sakata, T.; Nguyen, L.; Zhang, X.; et al. Single rhodium atoms anchored in micropores for efficient transformation of methane under mild conditions. *Nat. Commun.* **2018**, *9*, 1–11. [[CrossRef](#)]



© 2020 by the authors. Licensee MDPI, Basel, Switzerland. This article is an open access article distributed under the terms and conditions of the Creative Commons Attribution (CC BY) license (<http://creativecommons.org/licenses/by/4.0/>).